

See discussions, stats, and author profiles for this publication at: <https://www.researchgate.net/publication/319133120>

# Mueller Matrix Fluorescence Spectroscopy for Probing Self-Assembled Peptide Based Hybrid Supramolecular Structure and Orientation

Article in *The Journal of Physical Chemistry C* · August 2017

DOI: 10.1021/acs.jpcc.7b06725

CITATIONS

8

READS

424

5 authors, including:



**Krishnendu Maji**

Indian Institute of Science Education and Research Kolkata

19 PUBLICATIONS 103 CITATIONS

[SEE PROFILE](#)



**Sudipta Saha**

Indian Institute of Science Education and Research Kolkata

17 PUBLICATIONS 106 CITATIONS

[SEE PROFILE](#)



**Rajib Dey**

National University of Ireland, Galway

21 PUBLICATIONS 132 CITATIONS

[SEE PROFILE](#)



**Nirmalya Ghosh**

Indian Institute of Science Education and Research Kolkata

225 PUBLICATIONS 3,880 CITATIONS

[SEE PROFILE](#)

Some of the authors of this publication are also working on these related projects:




Emergence of robust waveguiding properties and Fano resonances in self assembled dipeptide microstructures [View project](#)



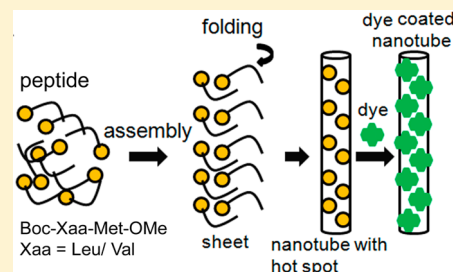
Image processing algorithms [View project](#)

# Mueller Matrix Fluorescence Spectroscopy for Probing Self-Assembled Peptide-Based Hybrid Supramolecular Structure and Orientation

Krishnendu Maji,<sup>†</sup> Sudipta Saha,<sup>‡</sup> Rajib Dey,<sup>‡</sup> Nirmalya Ghosh,<sup>\*,‡</sup> and Debasish Halder<sup>\*,†</sup> <sup>†</sup>Department of Chemical Sciences and <sup>‡</sup>Department of Physical Sciences, Indian Institute of Science Education and Research Kolkata, Mohanpur, Nadia, West Bengal 741246, India

## Supporting Information

**ABSTRACT:** Probing the assembly mechanism, orientation, shape, and structure function relationship of hybrid supramolecular materials is an outstanding challenge. In this regard, we have presented a novel method based on fluorescence spectroscopic Mueller matrix measurements and inverse analysis which can probe and quantify exclusive information on the molecular organization and orientation via a set of newly defined fluorescence anisotropy parameters, namely, fluorescence diattenuation and polarizance. A new dipeptide motif Boc-Xaa-Met-OMe (Xaa = Val/Leu) containing leucine, valine, and methionine forms a kink like structure and self-associates to form a twisted sheet like structure by multiple intermolecular N–H...O hydrogen bonds and finally grown to form supramolecular nanotubes having a diameter ca. 10 Å. Thus, the methionine sulfurs of peptide molecules are arranged helically along the tubes, work as a hot spot, and help to stabilize the electron deficient paint TB-NDI around the tube. The fluorescence Mueller matrix polarimetry and inverse analysis offers insight on the molecular organization and orientation of the achiral fluorescent dye molecules around the supramolecular nanotube from the chiral dipeptide. This method is promising for characterization of complex hybrid materials.



matrix to probe and quantify the organizational anisotropy related to morphological changes of a supramolecular hybrid. Fluorescence spectroscopy is a well-established technique widely explored for the characterization of diverse systems, ranging from chemical to physical, biological, and complex materials structures. The polarization properties of fluorescence contain potentially valuable information on the chemical structure, molecular organization, and local environment of the fluorophores, which is studied using the so-called fluorescence polarization anisotropy parameter (defined as the ratio of the polarized fluorescence component to the total intensity). Conventionally, the fluorescence anisotropy parameter is determined by detecting the co- and the crossed polarized components of the emitted fluorescence intensity using linear polarization excitation. Note that, in the context of optical response, the terminology “anisotropy” per se refers to anisotropic polarizability of matter, which originates from either anisotropic organization of otherwise isotropic molecular dipole moments or from intrinsically anisotropic molecular dipole moments. The measured fluorescence anisotropy parameter, on the other hand, is contributed by the depolarization (loss of degree of polarization) effects of fluorescence in addition to the “true” anisotropy effects. Depolarization of fluorescence arises due to several factors, e.g., the fast rotational diffusion of

## INTRODUCTION

Self-assembly of peptide motifs to fabricate supramolecular nanotubes is a popular field of interdisciplinary research due to their wide applications in biology and material sciences.<sup>1–6</sup> Moreover, the peptide motifs have structural and functional versatility, have biocompatibility, and are economical to form supramolecular nanotubes.<sup>7–10</sup> In this regard, designer cyclic peptides having a flat conformation and that stack to create cylindrical nanotubes are highly explored.<sup>11–14</sup> Over past few years, the tubular supramolecular nanotubes from the diphenylalanine motif has been extensively studied due to its remarkable physical and chemical stability<sup>15</sup> and unique mechanical,<sup>16–18</sup> electrical,<sup>19,20</sup> and optical<sup>21</sup> properties. Görbitz has reported the crystal structure of the tube<sup>22</sup> and Gazit et al. have used the diphenylalanine tubular supramolecular nanotubes as a template to cast silver nanowires.<sup>23</sup> Serpell et al. have reported the structure of cross- $\beta$  tapes and tubes formed by an octapeptide.<sup>24</sup> Recently, we have reported the fabrication of a supramolecular tubular host and supramolecular nanotubes.<sup>25</sup> However, most of the reported motifs contain aromatic amino acids and thus are easy to probe.

Probing the intermolecular interactions in supramolecular hybrid materials is highly important.<sup>26</sup> However, lack of direct probing techniques is the main stumbling block to study the molecular orientation, shape, and structure function relationship in such supramolecular systems. We have used a novel approach based on the fluorescence spectroscopic Mueller

matrix to probe and quantify the organizational anisotropy related to morphological changes of a supramolecular hybrid.

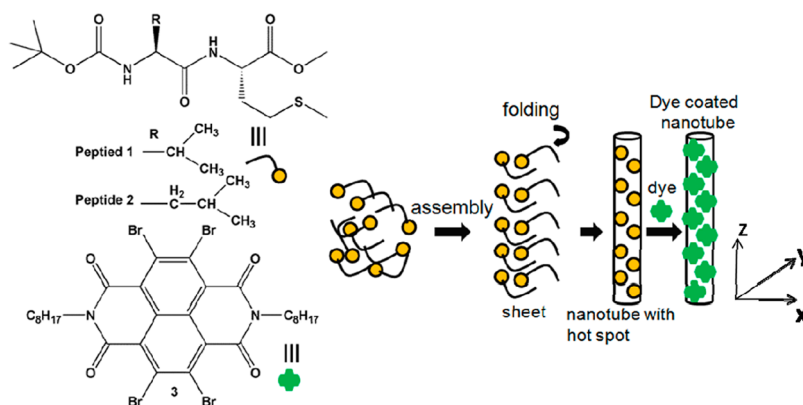
Fluorescence spectroscopy is a well-established technique widely explored for the characterization of diverse systems, ranging from chemical to physical, biological, and complex materials structures. The polarization properties of fluorescence contain potentially valuable information on the chemical structure, molecular organization, and local environment of the fluorophores, which is studied using the so-called fluorescence polarization anisotropy parameter (defined as the ratio of the polarized fluorescence component to the total intensity). Conventionally, the fluorescence anisotropy parameter is determined by detecting the co- and the crossed polarized components of the emitted fluorescence intensity using linear polarization excitation. Note that, in the context of optical response, the terminology “anisotropy” per se refers to anisotropic polarizability of matter, which originates from either anisotropic organization of otherwise isotropic molecular dipole moments or from intrinsically anisotropic molecular dipole moments. The measured fluorescence anisotropy parameter, on the other hand, is contributed by the depolarization (loss of degree of polarization) effects of fluorescence in addition to the “true” anisotropy effects. Depolarization of fluorescence arises due to several factors, e.g., the fast rotational diffusion of

Received: July 9, 2017

Revised: August 15, 2017

Published: August 15, 2017

**Scheme 1. Compounds 1, 2, and 3 and the Schematic Presentation of Supramolecular Nanotubes Formation and Processing of Nanotubes with Organic Dye<sup>a</sup>**



<sup>a</sup>The yellow circles are methionine sulphur atoms.

fluorophores, random orientation of the fluorophore molecules, the radiation less energy transfer among fluorophores, and other extrinsic causes such as multiple scattering effects. The fluorescence anisotropy determined using conventional approach thus reflects “lumped” effects arising from several simultaneously occurring polarizing/depolarizing interactions taking place during the fluorescence emission process. Yet, for many applications, it is desirable to extract and quantify exclusive information on the anisotropic molecular orientation and organization. Hence, a more encompassing polarimetric approach is needed that can capture complete information on the different polarizing and depolarizing interactions of fluorescence and can decouple the contributions of the individual effects. The Mueller matrix is a  $4 \times 4$  real intensity matrix that transforms any incoming Stokes vector (a  $4 \times 1$  real vector describing the state of polarization of light through measurable intensities) into another one and fully characterize the polarization properties of the sample under analysis.<sup>27</sup> However, such a matrix is conventionally defined for processes like reflection, refraction, and elastic scattering. Such Mueller matrix measurements and analysis are traditionally used to extract and quantify “bulk” (macroscopic) anisotropy properties of a medium. Adaptation of Mueller matrix formalism toward fluorescence spectroscopy may potentially address the more challenging problem of extraction and quantification of information on ‘intrinsic’ anisotropy originating from anisotropic molecular orientation and organization at the microscopic level. Recently, we and others have extended the theoretical framework of the Mueller matrix to describe polarization transformation in the case of fluorescence.<sup>28,29</sup> Here, we describe the use of such a generalized and encompassing polarimetric method on fluorescence spectroscopic Mueller matrix measurements and inverse analysis to probe and quantify exclusive information on the molecular orientation and organization of hybrid materials, that of the supramolecular nanotubes of Boc-Xaa-Met-OMe (Xaa = Val/Leu) and TB-NDI. The signatures of the preferential orientation and organization of the molecules manifested as differential excitation and emission of fluorescence for orthogonal polarizations (both linear and circular polarizations) and were characteristically encoded in the various elements of the fluorescence spectroscopic Mueller matrix. The corresponding information could be successfully gleaned through Mueller matrix inverse analysis and quantified via a set of newly defined

fluorescence anisotropy metrics, namely, fluorescence diattenuation (differential excitation of fluorescence by orthogonal polarizations) and fluorescence polarizance (differential emission of fluorescence by orthogonal polarizations).

We are looking for supramolecular nanotubes from self-assembly of stimuli responsive peptides and peptide mimetics.<sup>30,31</sup> We have discussed the sonication induced fiber like supramolecular nanotubes formation from self-assembly of peptide.<sup>32</sup> Herein, we have synthesized a series of dipeptides containing L-Leu, L-Val, and L-Met with the assumption that the peptide may adopt an extended structure and self-assembled by intermolecular hydrogen bonds to form fiber like supramolecular nanotubes (Scheme 1). The organization of Met sulphurs in supramolecular nanotubes will be interesting and can work as a hot spot to stabilize an electron deficient substrate. The dipeptide has no chromophore system. So, a substrate with chromophore will be helpful for spectroscopic studies. We incorporate organic dye 2,3,6,7-tetrabromo naphthalene diimide (TB-NDI) as the substrate (Scheme 1). We propose that the sulphurs of L-methionine residues can form a complex with an electron deficient substrate and thus develops processable supramolecular nanotubes (Scheme 1).

## EXPERIMENTAL SECTION

**Synthesis of Peptides. Synthesis of Boc-Val-OH.** L-Valine (1.17 g, 10 mmol) was taken in a mixture of dioxane (20 mL), water (10 mL), and 1 M NaOH (10 mL). The resulting solution was stirred and cooled in an ice-water bath. Then di-*tert*-butylpyrocarbonate (2.6 g, 12 mmol) was added into it, and stirring was continued at room temperature for 6 h. After that, the solution was concentrated under vacuum to about 10–15 mL, cooled in an ice–water bath, and covered with a layer of ethyl acetate (about 50 mL). The mixture was acidified with a dilute solution of KHSO<sub>4</sub> to pH 2–3, and the aqueous phase was extracted with ethyl acetate. This operation was done repeatedly. The ethyl acetate extract was pooled, washed with water, and dried over anhydrous Na<sub>2</sub>SO<sub>4</sub>. The solution was evaporated under vacuum to obtain a waxy solid product. Yield 1.52 g (7 mmol, 70%).

<sup>1</sup>H NMR (400 MHz, DMSO-*d*<sub>6</sub>,  $\delta$  in ppm): 12.38 [br, 1H, COOH], 6.87–6.85 [br, 1H, Boc NH], 3.75–3.74 [m, 1H, Val C <sup>$\alpha$</sup> H], 1.95–1.93 [m, 1H, val C <sup>$\beta$</sup> H], 1.45 [s, 9H, Boc CH<sub>3</sub>], 0.83–0.80 [m, 6H, val 2CH<sub>3</sub>]. <sup>13</sup>C NMR (100 MHz, DMSO-

$d_6$ ,  $\delta$  in ppm): 173.5, 155.7, 77.9, 59.1, 29.4, 28.2, 19.1, 18.1. Mass spectra:  $m/z$ : 240.17,  $[M + Na]^+$ ;  $M_{\text{calcd}}$ : 217.26.

**Synthesis of Boc-Val-Met-OMe 1.** Boc-Val-OH (1.52 g, 7 mmol) was dissolved in 20 mL of dry DCM in an ice-water bath. H-Met-OMe was isolated from 2.7 g (14 mmol) of the corresponding methyl ester hydrochloride by neutralization and subsequent extraction with ethyl acetate, and ethyl acetate extract was concentrated to 10 mL. It was then added to the reaction mixture, followed by immediate addition of 1.44 g (7 mmol) of dicyclohexyl carbodiimide (DCC) and 0.95 g (7 mmol) of HOBt. The reaction mixture was allowed to come to room temperature and stirred for 48 h. After that, DCM was evaporated, and the residue was dissolved in ethyl acetate (60 mL), and dicyclohexyl urea (DCU) was filtered off. The organic layer was washed with 2 M HCl (3  $\times$  50 mL), brine (2  $\times$  50 mL), 1 M sodium carbonate (3  $\times$  50 mL), and again with brine (2  $\times$  50 mL) and dried over anhydrous sodium sulfate. The solution was evaporated under vacuum to obtain dipeptide (1) as a white solid. The product was purified by silica gel (100–200 mesh) using *n*-hexane/ethyl acetate (3:1) as eluent. Yield 1.95 g (5.40 mmol, 77.14%).

$^1\text{H}$  NMR (400 MHz,  $\text{CDCl}_3$ ,  $\delta$  in ppm): 6.62–6.60 [br, 1H, NH], 5.05–5.03 [br, 1H, Boc NH], 4.70–4.69 [m, 1H, Val  $\text{C}^\alpha\text{H}$ ], 3.99–3.79 [m, 1H, Met  $\text{C}^\alpha\text{H}$ ], 3.70 [s, 3H, OMe], 2.49–2.47 [m, 2 H, Met,  $\text{C}^\beta\text{H}$ ], 2.14–2.11 [m, 2 H, Met  $\text{C}^\gamma\text{H}$ ], 2.07 [s, 3H,  $-\text{SCH}_3$ ], 1.42 [s, 9H, Boc  $\text{CH}_3$ ], 1.40–1.38 [m, 1H, Val  $\text{C}^\beta\text{H}$ ], 0.96–0.90 [m, 6H, Val,  $2\text{CH}_3$ ].  $^{13}\text{C}$  NMR (100 MHz,  $\text{CDCl}_3$ ,  $\delta$  in ppm): 172.0, 171.5, 155.5, 80.0, 60.0, 52.5, 51.4, 31.4, 30.7, 29.8, 28.2, 19.1, 15.4. Mass spectra:  $m/z$ : 385.07;  $[M + Na]^+$ ; 401.07  $[M + K]^+$ ;  $M_{\text{calcd}}$ : 362.19.

**Synthesis of Boc-Leu-OH.** L-Leucine (1.31 g, 10 mmol) was taken in a mixture of dioxane (20 mL), water (10 mL), and 1 M NaOH (10 mL). The resulting solution was stirred and cooled in an ice-water bath. Then di-*tert*-butylpyrocarbonate (2.6 g, 12 mmol) was added into it, and stirring was continued at room temperature for 6 h. After that, the solution was concentrated under vacuum to about 10–15 mL, cooled in an ice-water bath, and covered with a layer of ethyl acetate (about 50 mL). The mixture was acidified with a dilute solution of  $\text{KHSO}_4$  to pH 2–3, and the aqueous phase was extracted with ethyl acetate. This operation was done repeatedly. The ethyl acetate extract was pooled, washed with water, and dried over anhydrous  $\text{Na}_2\text{SO}_4$ . The solution was evaporated under vacuum to obtain a waxy solid product. Mass spectra:  $m/z$ : 254.144,  $[M + Na]^+$ ;  $M_{\text{calcd}}$ : 231.15. Yield 1.62 g (7 mmol, 70%).

$^1\text{H}$  NMR (400 MHz,  $\text{DMSO}-d_6$ ,  $\delta$  in ppm): 12.36 [b, 1H, COOH], 7.03–7.01 [d, 1H,  $J = 8$  Hz, Leu(1) NH], 3.91–3.87 [m, 1H, Leu(1)  $\text{C}^\alpha\text{H}$ ], 1.54–1.50 [m, 1H, Leu(1)  $\text{C}^\beta\text{H}$ ], 1.40–1.39 [m, 2H, Leu(1)  $\text{C}^\gamma\text{H}$ ], 1.37 [s, 9H, Boc], 0.87–0.82 [m, 6H, Leu(1),  $2\text{xCH}_3$ ].  $^{13}\text{C}$  NMR (100 MHz,  $\text{DMSO}-d_6$ ,  $\delta$  in ppm): 174.15, 155.64, 77.92, 51.78, 28.24, 24.38, 22.90, 21.23.

**Synthesis of Boc-Leu-Met-OMe 2.** Boc-Leu-OH (1.62g, 7 mmol) was dissolved in 20 mL of dry DCM in an ice-water bath. H-Met-OMe was isolated from 2.7 g (14 mmol) of the corresponding methyl ester hydrochloride by neutralization and subsequent extraction with ethyl acetate, and ethyl acetate extract was concentrated to 10 mL. It was then added to the reaction mixture, followed by immediate addition of 1.44 g (7 mmol) of dicyclohexyl carbodiimide (DCC) and 0.95 g (7 mmol) of HOBt. The reaction mixture was allowed to come to room temperature and stirred for 48 h. After that, DCM was evaporated, and the residue was dissolved in ethyl acetate (60 mL), and dicyclohexyl urea (DCU) was filtered off. The organic

layer was washed with 2 M HCl (3  $\times$  50 mL), brine (2  $\times$  50 mL), 1 M sodium carbonate (3  $\times$  50 mL), and brine (2  $\times$  50 mL) and dried over anhydrous sodium sulfate. The solution was evaporated under vacuum to obtain dipeptide (2) as a white solid. The product was purified by silica gel (100–200 mesh) using *n*-hexane/ethyl acetate (3:1) as eluent. Yield 2.01g (5.55 mmol, 79.32%).

$^1\text{H}$  NMR (400 MHz,  $\text{CDCl}_3$ ,  $\delta$  in ppm): 6.78–6.76 [br, 1H, NH], 4.95 [br, 1H, Boc NH], 4.68–4.63 [m, 1H, Leu(1)  $\text{C}^\alpha\text{H}$ ], 4.07 [br, 1H, Met(2)  $\text{C}^\alpha\text{H}$ ], 3.71 [s, 3H,  $-\text{OCH}_3$ ], 2.48–2.45 [m, 4H, Met(2)  $\text{C}^\beta\text{H}$  and  $\text{C}^\gamma\text{H}$ ], 2.05 [s, 3H,  $-\text{SCH}_3$ ], 1.96–1.92 [m, 1H, Leu(1)  $\text{C}^\gamma\text{H}$ ], 1.65–1.59 [m, 2H, Leu(1)  $\text{C}^\beta\text{H}$ ], 1.4103 [s, 9H, Boc  $\text{CH}_3$ ], 0.9237–0.8912 [m, 6H, Leu(1)  $2\text{xCH}_3$ ].  $^{13}\text{C}$  NMR (100 MHz,  $\text{DMSO}-d_6$ ,  $\delta$  in ppm): 173.61, 173.36, 156.92, 54.33, 53.76, 52.62, 42.13, 32.86, 31.02, 29.51, 25.92, 24.10, 23.28, 16.66. Mass spectra:  $m/z$ : 377.48,  $[M + H]^+$ ; 399.44,  $[M + Na]^+$ ;  $M_{\text{calcd}}$ : 376.2.

**NMR Spectroscopy.** All NMR studies were carried out on a Bruker AVANCE 500 MHz spectrometer at 278 K. Compound concentrations were in the range 1–10 mM in  $\text{CDCl}_3$  and  $(\text{CD}_3)_2\text{SO}$ .

**FT-IR Spectroscopy.** All reported solid-state FTIR spectra were obtained with a PerkinElmer Spectrum RX1 spectrophotometer with the KBr disk technique.

**Mass Spectrometry.** Mass spectra were recorded on a Q-ToF Micro YA263 high-resolution (Waters Corporation) mass spectrometer by positive-mode electrospray ionization.

**Single Crystal X-ray Structure Analysis.** Colorless crystals of peptides 1 and 2 suitable for X-ray diffraction studies were obtained from their respective methanol–water solution by slow evaporation. Single-crystal X-ray analysis of peptides 1 and 2 were recorded on a Bruker high resolution X-ray diffractometer instrument. The structures were solved by a direct method and refined by least-squares calculations on  $F^2$  for all independent reflections (SHELXL-2013). Crystal data of peptide 1:  $\text{C}_{16}\text{H}_{30}\text{N}_2\text{O}_5\text{S}$ ,  $M_w = 362.48$ , orthorhombic,  $P2_12_12_1$ ,  $a = 11.2433(2)$  Å,  $b = 20.6448(3)$  Å,  $c = 36.2792(5)$  Å,  $V = 8421(2)$  Å<sup>3</sup>,  $Z = 16$ ,  $\text{dm} = 1.144$  Mg  $\text{m}^{-3}$ ,  $K = 100$ ,  $R1 = 0.0448$ , and  $wR2 = 0.1217$  for 13423 data with  $I > 2\sigma(I)$ . Crystal data of peptide 2:  $\text{C}_{17}\text{H}_{32}\text{N}_2\text{O}_5\text{S}$ ,  $M_w = 376.51$ , orthorhombic,  $P2_12_12_1$ ,  $a = 21.584(8)$  Å,  $b = 37.476(13)$  Å,  $c = 10.955(4)$  Å,  $V = 8861(6)$  Å<sup>3</sup>,  $Z = 16$ ,  $\text{dm} = 1.129$  Mg  $\text{m}^{-3}$ ,  $K = 293$ ,  $R1 = 0.1108$ , and  $wR2 = 0.3142$  for 16401 data with  $I > 2\sigma(I)$ . Intensity data were collected with Mo  $K\alpha$  radiation using Bruker APEX-2 CCD diffractometer. Data were processed using the Bruker SAINT package, and the structure solution and refinement procedures were performed using SHELX97 and deposited at CCDC with reference 1044920 and 983309 for peptides 1 and 2, respectively.

**UV/vis Spectroscopy.** UV/vis absorption spectra were recorded on a UV/vis spectrophotometer (Hitachi).

**Circular Dichroism (CD) Spectroscopy.** CD studies of the peptides in solid state and in methanol have been carried out on a JASCO J-815–150S instrument at a temperature of 25 °C.

**Mueller Matrix Fluorescence Spectroscopy.** The home-made experimental fluorescence Mueller matrix setup (experimental system subsequently shown in Figure 3) is capable of recording the 16-element Mueller matrix (4  $\times$  4). The system comprises a 405 nm diode laser as an excitation source (Pegasus, Shanghai, China), a polarization state generator (PSG) unit, and a polarization state analyzer (PSA) unit to generate and analyze the required polarization states coupled to



a CCD spectrometer (Shamrock imaging spectrograph, SR-303i-A, ANDOR technology) for spectrally resolved signal detection. The PSG unit consists of a linear polarizer (P1, LPVIS100, Thorlabs, USA) oriented horizontally followed by a rotatable achromatic quarter wave retarder (Q1, AQWP05M-600, Thorlabs, U.S.A.) mounted on a computer controlled rotational mount (PRM1/M-27E, Thorlabs, USA). The PSA unit also contains a similar arrangement of a fixed linear polarizer (P2, oriented vertically) and rotatable achromatic quarter wave retarder (Q2), but positioned in the reverse order. The microscope objective (MO) was used to focus the light into the sample and also to collect the emitted fluorescence signal from the sample. The fluorescence signal from the sample was collected, passed through the PSA, and relayed to the spectrally resolved signal detection unit (CCD/Spectrograph). The filter (F) used in this setup is a cutoff filter which is used to block the excitation wavelength ( $\lambda_{\text{ex}} = 405 \text{ nm}$ ) from reaching the detector so that only the emitted fluorescence spectra is recorded for the wavelength range 450–800 nm with a resolution of 1 nm.

The  $4 \times 4$  spectral Mueller matrix was constructed by combining 16 spectrally resolved intensity measurements (spectra). In this approach, four optimized elliptical polarization states are generated in the PSG unit, and for each of the PSG states, the analyzer states are measured for four optimized elliptical states. The four elliptical polarization states are generated in the PSG unit by sequentially changing the orientation angle of the fast axis of Q<sub>1</sub> to four angles ( $\theta = 35^\circ, 70^\circ, 105^\circ, \text{ and } 140^\circ$ ) w.r.t. the axis of P<sub>1</sub>. Out of these four elliptical PSG states (defined by the Stokes vector ( $4 \times 1$ )), a  $4 \times 4$  generator matrix ( $W$ ) is constructed by grouping them in the form of four column vectors. In a similar manner, the four elliptical analyzer basis states are obtained by changing the fast axis of Q<sub>2</sub> to the corresponding four angles ( $\theta = 35^\circ, 70^\circ, 105^\circ, \text{ and } 140^\circ$ ). Again the analyzer states are grouped in the form of row vectors to construct the  $4 \times 4$  analyzer matrix ( $A$ ). These PSG and PSA states are optimized for reducing the errors in the construction of Mueller matrix. Theoretical optimization of the orientation angles ( $\theta$ ) were performed to obtain the optimal generator ( $W$ ) and the analyzer ( $A$ ) matrices that would lead to minimal propagation of errors while constructing the Mueller matrix using the 16 polarization resolved intensity measurements. A general criterion for this has previously been suggested to be based on optimization of the so-called “condition number”, defined as the ratio of the smallest to the largest singular values of the individual square matrices  $W$  and  $A$ .<sup>33</sup> The orientation angles of the quarter waveplates ( $\theta = 35^\circ, 70^\circ, 105^\circ, \text{ and } 140^\circ$ ) were decided based on this.<sup>33</sup>

The 16 sequential intensity measurements (at any wavelength) are grouped in  $4 \times 4$  matrix ( $M_i$ ), which is related to  $A$  and  $W$  matrices and the sample Mueller matrix  $M$  via the relation:

$$M_i = AMW \quad (1)$$

The sample Mueller matrix ( $M$ ) can then be determined using the known forms of  $A$  and  $W$  matrices as

$$M = A^{-1}M_iW^{-1} \quad (2)$$

Hence, in principle,  $M$  can be determined from experimental  $M_i$  using the theoretical form of  $A$  and  $W$ . However, this is confounded by the fact that  $W(\lambda)$  and  $A(\lambda)$  matrices may significantly vary with wavelength  $\lambda$  due to nonideal behavior of the polarizing optics over the wavelength range. This has been

taken care of by the so-called eigen-value calibration method (ECM) which takes care of the spectral polarization response of  $W(\lambda)$  and  $A(\lambda)$ . ECM determines the exact experimental forms of  $W(\lambda)$  and  $A(\lambda)$  matrices by performing measurements on a set of known calibrating samples (pure diattenuator (polarizer) and retarder (waveplate)). ECM offers high accuracy ( $\sim 0.01$  in normalized matrix elements) over the entire spectra region (450–800 nm).<sup>33,34</sup>

**Inverse Analysis of the Fluorescence Spectroscopic Mueller Matrix.** In order to build our inverse analysis model, we write the recorded fluorescence Mueller matrix as the product of three basis matrices such that  $R = M_1M_dM_0$ .<sup>28,29</sup> Here, the matrix  $M_d$  accounts for the depolarization effects of fluorescence that arises due to random orientation of the fluorophores and other extrinsic causes. The corresponding polarization transfer matrix is given by the following form:<sup>28</sup>

$$M_d = \begin{pmatrix} a - b \sin^2 \phi & -b \sin^2 \phi & 0 & 0 \\ -b \sin^2 \phi & b(1 + \cos^2 \phi) & 0 & 0 \\ 0 & 0 & 2b \cos \phi & 0 \\ 0 & 0 & 0 & 2c \cos \phi \end{pmatrix} \quad (3)$$

where  $\phi$  is the scattering angle, the parameters  $a$  and  $b$  are function of the angle between the emission dipole and the azimuth of the polarization of the exciting beam, and  $c$  is related to optical activity. The matrices  $M_0$  and  $M_1$  account for the amplitude anisotropies associated with the ground and the excited molecular states of fluorophore molecules, respectively. Since the fluorescence is associated with randomization of field vector, the phase anisotropies are usually neglected in the two matrices. Hence, the mathematical forms of the matrices ( $M_0$  and  $M_1$ ) can be given as<sup>35</sup>

$$M_0 = \begin{pmatrix} 1 & m_0 & n_0 & p_0 \\ m_0 & r_0' & 0 & 0 \\ n_0 & 0 & r_0'' & 0 \\ p_0 & 0 & 0 & r_0''' \end{pmatrix}; \quad M_1 = \begin{pmatrix} 1 & m_1 & n_1 & p_1 \\ m_1 & r_1' & 0 & 0 \\ n_1 & 0 & r_1'' & 0 \\ p_1 & 0 & 0 & r_1''' \end{pmatrix} \quad (4)$$

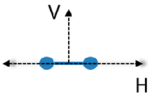
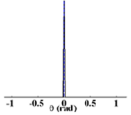
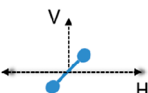
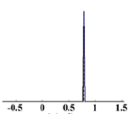
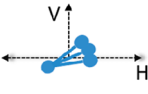
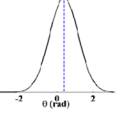
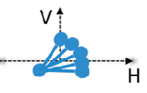
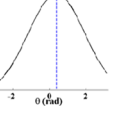
Here, the parameters ( $m_0, n_0, p_0; m_1, n_1, p_1$ ) are the amplitude anisotropy parameters. Specifically  $m_0, n_0, p_0$  correspond to horizontal ( $0^\circ$ )/vertical ( $90^\circ$ ) linear,  $\pm 45^\circ$  linear and circular diattenuation (differential excitation of fluorescence with orthogonal polarization) respectively. Similarly  $m_1, n_1, p_1$  correspond to horizontal ( $0^\circ$ )/vertical ( $90^\circ$ ) linear,  $\pm 45^\circ$  linear and circular polarizance (differential emission of fluorescence with orthogonal polarization) respectively.

Using the forms of the above matrices, the elements of the resultant fluorescence Mueller matrix can be determined, and by using few algebraic manipulations and approximations, the following useful relations can be obtained:

$$\begin{aligned} R_{12}/R_{11} &\approx m_0; & R_{13}/R_{11} &\approx n_0 \\ R_{21}/R_{11} &\approx m_1; & R_{31}/R_{11} &\approx n_1 \\ R_{14}/R_{11} &\approx p_0; & R_{41}/R_{11} &\approx p_1 \end{aligned} \quad (5)$$

Thus, the elemental ratios  $R_{12}/R_{11}$ ,  $R_{13}/R_{11}$ , and  $R_{14}/R_{11}$  directly yield the horizontal ( $0^\circ$ )/vertical ( $90^\circ$ ) linear,  $\pm 45^\circ$

**Table 1. Illustration of Representative Angular Molecular Distribution Function  $f(\theta)$  for Different Orientations of Fluorophore Molecules and the Calculated Values of  $R_{12}$ ,  $R_{13}$ ,  $\alpha_L$ ,  $\theta_{ex}$ , and  $\Delta\theta_{ex}$  Using the Theoretical Model Given by eqs 8–11<sup>a</sup>**

Orientation of fluorescent molecule	Molecular angular distribution function $f(\theta)$	$R_{12}$	$R_{13}$	$\alpha_L$	$\theta_{ex}$	$\Delta\theta_{ex}$
		1	0	1	0	0
		0	1	1	$\pi/4$	0
		-0.24	0.56	0.61	$\pi/8$	$\pi/4$
		-0.36	0.19	0.41	$\pi/8$	$\pi/2$

<sup>a</sup>The dumbbell represents the 2D orientations of fluorescent w.r.t. the horizontal (H) and vertical (V) polarization axes.

linear, and circular diattenuation (differential excitation of fluorescence), respectively. Similarly,  $R_{21}/R_{11}$ ,  $R_{31}/R_{11}$ , and  $R_{41}/R_{11}$  yield the horizontal ( $0^\circ$ )/vertical ( $90^\circ$ ) linear, and circular polarizance (differential emission of fluorescence), respectively.

We then define the following important anisotropy parameters from the resultant fluorescence Mueller matrix ( $\mathbf{R}$ ):

$$\alpha_T = \frac{\sqrt{R_{12}^2 + R_{13}^2 + R_{14}^2}}{R_{11}}; \quad \alpha_L = \frac{\sqrt{R_{12}^2 + R_{13}^2}}{R_{11}}; \quad \alpha_C = \frac{R_{14}}{R_{11}} \quad (6)$$

$$\beta_T = \frac{\sqrt{R_{21}^2 + R_{31}^2 + R_{41}^2}}{R_{11}}; \quad \beta_L = \frac{\sqrt{R_{21}^2 + R_{31}^2}}{R_{11}}; \quad \beta_C = \frac{R_{41}}{R_{11}} \quad (7)$$

where  $\alpha_T$ ,  $\alpha_L$ , and  $\alpha_C$  are the total, linear, and circular fluorescence diattenuation, respectively, and  $\beta_T$ ,  $\beta_L$ , and  $\beta_C$  are the total, linear and circular polarizance, respectively. These parameters were extracted from the Fluorescence Mueller matrix  $\mathbf{R}$  (subsequently shown in Figure 5).<sup>29</sup>

**Relation between the Fluorescence Linear Diattenuation ( $\alpha_L$ ) and Linear Polarizance ( $\beta_L$ ) Parameters with Molecular Orientational Order.** Using the elements of the fluorescence Mueller matrix, the average fluorescent dipolar orientation angles for the ground ( $\theta_{ex}$ ) and the excited ( $\theta_{em}$ ) molecular states can be obtained as<sup>27</sup>

$$\theta_{ex} = \frac{1}{2} \tan^{-1} \left( \frac{R_{13}}{R_{12}} \right) \\ \theta_{em} = \frac{1}{2} \tan^{-1} \left( \frac{R_{31}}{R_{21}} \right) \quad (8)$$

In order to link the fluorescence linear diattenuation ( $\alpha_L$ ) and linear polarizance ( $\beta_L$ ) parameters with ground and excited state molecular orientational order, we define the molecular angular distribution function ( $f(\theta)$ ). This function includes information on the distribution of the orientation angles of the molecules with width  $\Delta\theta$  around the average fluorescent dipolar orientation angle ( $\theta_{ex}$  and  $\theta_{em}$ ). Using this function, the measured fluorescence intensity for excitation with a given polarization vector  $\mathbf{E}$  can be written as

$$I_H \propto \int_0^\pi |\boldsymbol{\mu} \cdot \mathbf{E}_H|^2 f(\theta) d\theta \propto \int_0^\pi \cos^2(\theta) f(\theta) d\theta \\ I_V \propto \int_0^\pi |\boldsymbol{\mu} \cdot \mathbf{E}_V|^2 f(\theta) d\theta \propto \int_0^\pi \sin^2(\theta) f(\theta) d\theta \\ I_{P/M} \propto \int_0^\pi |\boldsymbol{\mu} \cdot \mathbf{E}_{P/M}|^2 f(\theta) d\theta \propto \int_0^\pi \cos^2(\theta \pm \pi/4) f(\theta) d\theta \quad (9)$$

with

$$f(\theta) \propto e^{-(\theta - \theta_{ex/em})^2 / 2\Delta\theta_{ex/em}^2} \quad (10)$$

Here,  $\boldsymbol{\mu}$  is the molecular dipole moment in the ground state and  $I_{H/V}$  ( $I_{P/M}$ ) denotes the measured fluorescence intensities with horizontal/vertical ( $+45^\circ/-45^\circ$ ) linear polarization excitations. Depending upon the nature of the organization of the molecules, the specific functional form of  $f(\theta)$  can be chosen.<sup>36,37</sup> However, for the sake of generality, we have used a Gaussian distribution of the orientation angle centered around

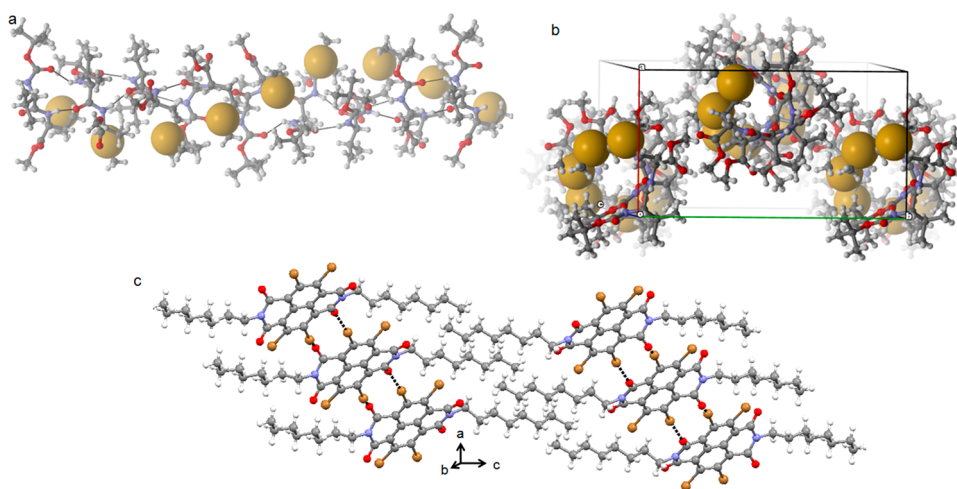


**Figure 1.** (a) Twisted sheet like assembly of dipeptide **1** and the helical arrangement of sulfur atoms (yellow balls). The intermolecular hydrogen bonds are shown as black dotted lines. (b) The top view and packing diagram of the twisted sheet showing parallel arrangement of peptide **1** nanotube like structures. (c) The complex sheet like structure of TB-NDI **3** through the C=O...Br halogen bond and hydrophobic interactions between *n*-octyl moieties.

$\theta_{\text{ex}}$  (or  $\theta_{\text{em}}$ , which can be determined from experimental Mueller matrix using eq 8) with a standard deviation of the orientation angle distribution ( $\Delta\theta_{\text{ex}}$  or  $\Delta\theta_{\text{em}}$ ). As is evident, the set of intensities in eq 9 represent the differential excitation of fluorescence by orthogonal linear polarizations. The corresponding fluorescence linear diattenuation ( $\alpha_{\text{L}}$ ) parameter encoding the excitation anisotropy of the ground state can therefore be formally related to the above intensity expressions as

$$\alpha_{\text{L}} = \sqrt{\frac{(I_{\text{H}} - I_{\text{V}})^2}{(I_{\text{H}} + I_{\text{V}})^2} + \frac{(I_{\text{P}} - I_{\text{M}})^2}{(I_{\text{P}} + I_{\text{M}})^2}} \quad (11)$$

The relation between the fluorescence linear polarizance ( $\beta_{\text{L}}$ ), encoding the emission anisotropy of the excited state, and the excited state molecular orientational order can be obtained in identical fashion (eqs 9–11). Here,  $\mu$  will be the excited state dipole moment and  $I_{\text{H/V}}$  ( $I_{\text{P/M}}$ ) will be the measured fluorescence intensities with horizontal/vertical (+45°/−45°) linear polarizations at the detection end. Inverse calculations on the Mueller matrix-derived  $\alpha_{\text{L}}$  and  $\beta_{\text{L}}$  parameters (taking the experimentally determined  $\theta_{\text{ex}}$  and  $\theta_{\text{em}}$  values) using eqs 9–11 can then be performed to obtain the standard deviation of the orientation angle distribution ( $\Delta\theta_{\text{ex}}$  or  $\Delta\theta_{\text{em}}$ ), which is a quantitative measure of the molecular orientational order.

In Table 1, we have illustrated the angular molecular distribution function and its relation with the molecular orientation ordering. It is evident from Table 1 that for perfect preferential linear organization or for high molecular order (shown in the first and the second row), the magnitudes of  $\alpha_{\text{L}}$  and  $\beta_{\text{L}}$  approach the limiting value of unity. Distribution of the orientation angles of the molecular dipoles (nonzero value of  $\Delta\theta$ ), on the other hand, leads to reduction in the magnitudes for the  $\alpha_{\text{L}}$  and  $\beta_{\text{L}}$  parameters (shown in the third and fourth row). A small value of  $\Delta\theta_{\text{ex}}$  (or  $\Delta\theta_{\text{em}}$ ) therefore corresponds to high molecular order, which leads to high magnitudes (approaching unity) of the  $\alpha_{\text{L}}$  and  $\beta_{\text{L}}$  parameters. A large value of  $\Delta\theta_{\text{ex}}$  (or  $\Delta\theta_{\text{em}}$ ), on the other hand, reflects lower molecular order leading to low magnitudes of the  $\alpha_{\text{L}}$  and  $\beta_{\text{L}}$  parameters. The magnitudes of the  $\alpha_{\text{L}}$  and  $\beta_{\text{L}}$  parameters therefore capture quantitative information on the rotation

invariant (independent of the laboratory reference frame) orientational order of the ground and the excited state molecular dipoles (respectively). This information on the molecular orientation order can be treated as an averaged information in space, over the whole molecular population probed by the excitation light in the steady state (time averaged) regime. Moreover, the orientation angle ( $\theta$ ) information obtained from fluorescence Mueller matrix measurement (like any other polarization resolved experiments) should necessarily be interpreted as a two-dimensional projection of the actual three-dimensional molecular orientation into the reference plane containing the laboratory polarization axes.

## RESULTS AND DISCUSSION

Target compounds were synthesized by conventional solution phase methods, purified, and characterized by  $^1\text{H}$  NMR,  $^{13}\text{C}$  NMR, FT-IR, and mass spectrometry (MS) analysis. X-ray crystallography sheds some light on molecular structure and self-assembly pattern of the dipeptides **1** and **2**. The torsion angle around the valine, leucine, and methionine residues appears to play a critical role in dictating the overall extended structure of dipeptides **1** and **2** (Supporting Information, Table 1). From the crystal structure of dipeptide **1**, it is evident that there are multiple cooperative intermolecular hydrogen bonds between Boc C=O and Val NH and Val C=O and Met NH to form and stabilize the supramolecular sheet like structure along the crystallographic *c* direction (Figure 1a). The sheet is twisted in nature as it is seen from the helically arranged sulfur atoms along the crystallographic *c* direction (Figure 1a). The supramolecular helical pitch is 32.74 Å and contains eight peptide **1** molecules. Thus, the top view of the higher order packing along the crystallographic *c* direction exhibits the tube like structure (Figure 1b). The diameter of the nanotube is about 10 Å and the diameter of the pore is about 6 Å. In higher order packing, the individual nanotube like structure further self-assembles by various noncovalent interactions along the crystallographic *b* direction (Figure 1b). From X-ray analysis, there are four molecules in the asymmetric unit of peptide **2**. The molecules are coupled by multiple cooperative intermolecular hydrogen bonds between Boc C=O and Leu NH

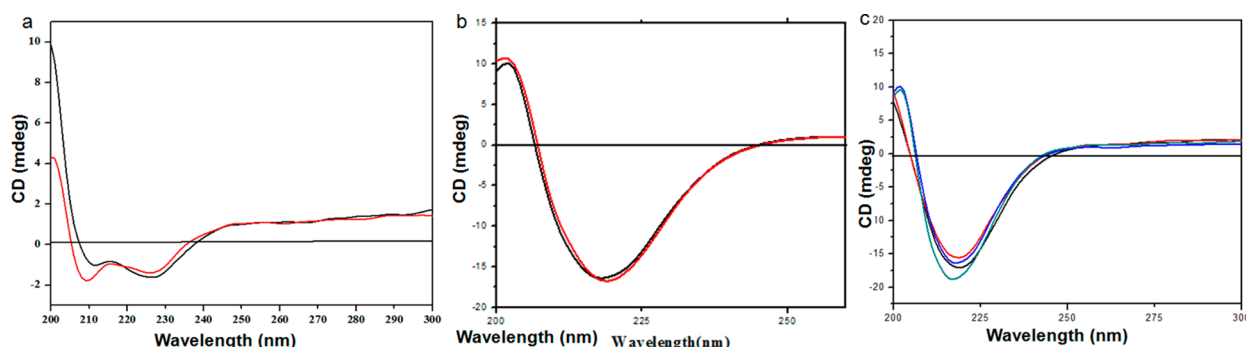


**Figure 2.** (a) CD spectra of dipeptides **1** (red) and **2** (black) in methanol ( $1 \times 10^{-6}$  M). (b) CD spectra of dipeptides **1** (red) and **2** (black) in methanol ( $1 \times 10^{-5}$  M). (c) CD spectra of dipeptide **1** and TB-NDI hybrid. Black, peptide **1** in solid state; red, peptide **1** and TB-NDI in solid state; blue, only peptide **1** in methanol; green, peptide **1** with TB-NDI in methanol.

and Leu C=O and Met NH that stabilize the supramolecular sheet like structure along the crystallographic *c* direction (Figure S1a). Finally the sheet has twisted geometry as it is evident from the helically arranged sulfur atoms along the crystallographic *c* direction (Figure S1a). From the top view of the peptide **2** twisted sheet, a nanotube like structure has appeared (Figure S1b,c). The hydrogen bonding parameters of peptides **1** and **2** are listed in the Supporting Information, Table 2. The sulphurs of L-methionine residues on the surface of the tube are like hot spots. The sulfur has lone pairs of electrons and can form a complex with the electron deficient substrate. We have utilized this possibility to decorate the tubes with organic dyes 2,3,6,7-tetrabromo naphthalene diimide (TB-NDI) **3**. Zhu and co-workers have reported the synthesis and X-ray crystal structure of TB-NDI **3**.<sup>38</sup> The TB-NDI exhibits backbone contortion in the central aromatic core, leading to a dimer structure by two intermolecular halogen bonds<sup>39</sup> between imide C=O and Br (Figure S2). The dimeric units are further self-assembled by two cooperative halogen bonding interactions to form a supramolecular sheet like structure (Figure 1c).

The typical UV/vis absorption spectra of the dipeptides **1** and **2** were studied as a function of concentration. Irrespective of hydrophobic Val/Leu side chains, the dipeptides exhibit same absorption bands at 225 and 280 nm due to the characteristic  $\pi-\pi^*$  transition (Figure S3). With the gradual increase in the concentration the dipeptides exhibit no shift in their respective absorption bands, but only the intensity of the band increases (Figure S3). The aggregation propensities of the reported dipeptides were further studied by circular dichroism (CD) spectroscopy. At low concentration the CD spectra exhibit general information on the secondary structure of the dipeptides. CD spectroscopy of dipeptide **1** in dilute methanol solution ( $1 \times 10^{-6}$  M) indeed shows a mostly helical pattern with strong negative Cotton effect centered on 210 and 226 nm (Figure 2a). For dipeptide **2** in dilute methanol solution ( $1 \times 10^{-6}$  M) the CD pattern does not change but the negative Cotton effect appears at 209 and 226 nm (Figure 2a). However, at high concentration ( $1 \times 10^{-5}$  M), for both the peptides the CD patterns change and exhibit negative Cotton effect at 216 nm, due to formation of aggregated structures (Figure 2b). The results indicate a similar self-assembly pattern of dipeptides **1** and **2** in solution. The aggregation propensities of the hybrid from TB-NDI and peptide nanotube were also studied by CD spectroscopy (Figure 2c). To avoid various structures, we have done these experiments at a higher concentration of peptides ( $1 \times 10^{-5}$  M). The solid as well as solution state (methanol) CD

spectroscopy of dipeptide **1** indeed show only one kind of aggregation pattern with a strong negative Cotton effect centered on 216 nm (Figure 2c). However, after addition of TB-NDI the CD pattern does not change (Figure 2c).

From FT-IR spectroscopy, for peptides **1** and **2** the intense peak at  $3328\text{ cm}^{-1}$  indicates the presence of strongly hydrogen-bonded NH groups (Figure S4 and S5b).<sup>40</sup> The peak at  $1752\text{ cm}^{-1}$  indicates the C = O stretching vibrations of saturated non hydrogen bonded methyl ester.<sup>40</sup> The amide I band at  $1650\text{ cm}^{-1}$  and amide II band at  $1525\text{ cm}^{-1}$  suggest that the peptides adopt a kink like conformation in the solid state. After addition of TB-NDI the FT-IR pattern does not change and there is no shift of the characteristic bands (Figure S4). Peptide **2** also exhibits the same result on treatment with TB-NDI as studied by CD and FT-IR spectroscopy (Figure S5). The results indicate that the aggregated peptide structures are uniform and very rigid.

**Fluorescence Mueller Matrix Studies.** The peptide **1** has an intrinsic propensity to form a rigid nanotube structure with sulfur atoms on the tube surface in a helical manner (established by X-ray crystal structure and other experimental methods). In order to obtain further information on the anisotropic molecular organization and orientation, fluorescence spectroscopic Mueller matrices were recorded from painted supramolecular helix from the assembly of a dipeptide and naphthalene-diimide (TB-NDI). For the fluorescence Mueller matrix study, the methanol solution of peptide **1** ( $1 \times 10^{-5}$  M) was sonicated for 10 min and allowed to settle for 30 min. To this solution,  $3\ \mu\text{L}$  of  $1 \times 10^{-3}$  M TB-NDI dye was added. The scheme of our fluorescence spectroscopic Mueller matrix measurements is shown in Figure 3. The experimental system (Figure 3) is capable of recording a full  $4 \times 4$  fluorescence spectroscopic Mueller matrix in the exact backscattering configuration (see the Experimental Section for the details of the experimental system). Briefly, the system employs excitation with the wavelength  $\lambda_{\text{ex}} = 405\text{ nm}$  of a diode laser, and subsequent recording of 16 polarization resolved fluorescence spectra (wavelength  $\lambda_{\text{em}} = 450\text{--}800\text{ nm}$ , 1 nm resolution) by sequential generation and analysis of four optimized elliptical polarization states. The polarization state generator (PSG) and the polarization state analyzer (PSA) units are used for sequential generation and analysis of four optimized elliptical polarization states. The 16 polarization resolved fluorescence spectra recorded using the spectrally resolved signal detection unit (CCD/spectrograph) are utilized to construct the  $4 \times 4$  fluorescence spectroscopic Mueller matrix.<sup>33</sup>



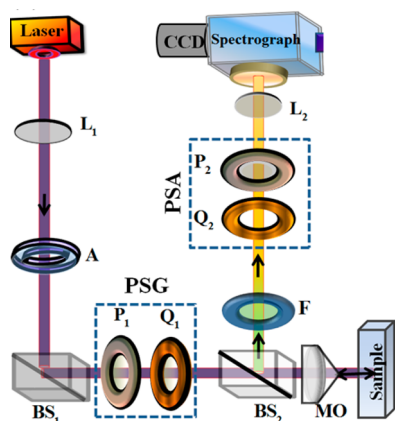


**Figure 3.** Schematic of the spectroscopic fluorescence Mueller matrix setup.  $L_1$ ,  $L_2$ : lenses; A: variable aperture;  $BS_1$  and  $BS_2$ : beam splitters; MO: microscope objective; F: long pass filter;  $P_1$  and  $P_2$ : linear polarizers;  $Q_1$  and  $Q_2$ : achromatic quarter wave retarders.  $P_1$  and  $Q_1$  form the polarization state generator (PSG) unit.  $P_2$  and  $Q_2$  form the polarization state analyzer (PSA) unit.

The spectroscopic fluorescence Mueller matrix  $\mathbf{R}$  recorded from TB-NDI is shown in Figure 4. Several interesting trends are apparent from the  $4 \times 4$  Mueller matrix. Even though the matrix appears complicated with nonzero values of the 16 elements, some qualitative understanding on the contributing polarimetry effects can be gained by inspecting the characteristic elements. The first element  $R_{11}$  (which represents unpolarized fluorescence spectra) shows a prominent peak around  $\sim 530$  nm, which is the characteristic fluorescence peak of TB-NDI. The spectral intensities of the diagonal elements are considerably weaker as compared to the  $R_{11}$  element ( $R_{22}$ ,  $R_{33}$ , and  $R_{44} \ll R_{11}$ ). In general, the diagonal elements of the Mueller matrix represent polarization preserving components for horizontal ( $0^\circ$ )/vertical ( $90^\circ$ ) linear polarizations,  $\pm 45^\circ$  linear polarizations, and right/left circular polarizations,

respectively. The weak intensity values of the diagonal elements thus underscore the overall strong depolarizing nature of the fluorescence. We note that these strong depolarization effects, which are not related to the “true” organizational anisotropy of the fluorophores, should contribute to the traditionally measured fluorescence anisotropy parameter.<sup>29</sup> Recording of a full  $4 \times 4$  fluorescence Mueller matrix thus enables proper interpretation and decoupling of depolarization from the actual anisotropy effects that are related to the preferential organization of fluorophore molecules (discussed subsequently). The elements  $R_{23}$ ,  $R_{24}$ ,  $R_{34}$ ,  $R_{32}$ ,  $R_{42}$ , and  $R_{43}$  of the recorded Mueller matrix  $\mathbf{R}$  represent phase retardation effects (differential phase between orthogonal linear or circular polarizations). While, the elements ( $R_{34}$ ,  $R_{43}$ ) and ( $R_{24}$ ,  $R_{42}$ ) carry information on the phase retardation between horizontal/vertical and  $+45^\circ/-45^\circ$  linear polarizations, respectively, the difference in the  $R_{23}$  and  $R_{32}$  elements encode information on phase retardation between left and right circular polarization states. Since the fluorescence process is inherently associated with strong dephasing effects, the intensity values corresponding to these retardance-carrying elements ( $R_{34}$ ,  $R_{43}$ ,  $R_{24}$  and  $R_{42}$  elements carrying linear retardance information and  $R_{23}$ ,  $R_{32}$  elements carrying circular retardance information) are also consequently quite weak and do not exhibit any notable spectral features (spectrally flat).

In contrast, the elements of first row and first column of the Mueller matrix show significant intensities with spectral features similar to the TB-NDI emission. As discussed previously, significant intensity values (and distinct spectral features) of these elements underscore the presence of the excitation and the emission anisotropies originating from preferential orientation and organization of the fluorophore molecules. Specifically, the elements  $R_{12}$ ,  $R_{13}$ , and  $R_{14}$  (in the first row, highlighted by blue color in Figure 4) encode excitation anisotropy (differential excitation of fluorescence by orthogonal linear and circular polarizations) of the ground state and the elements  $R_{21}$ ,  $R_{31}$ , and  $R_{41}$  (in the first column, highlighted by

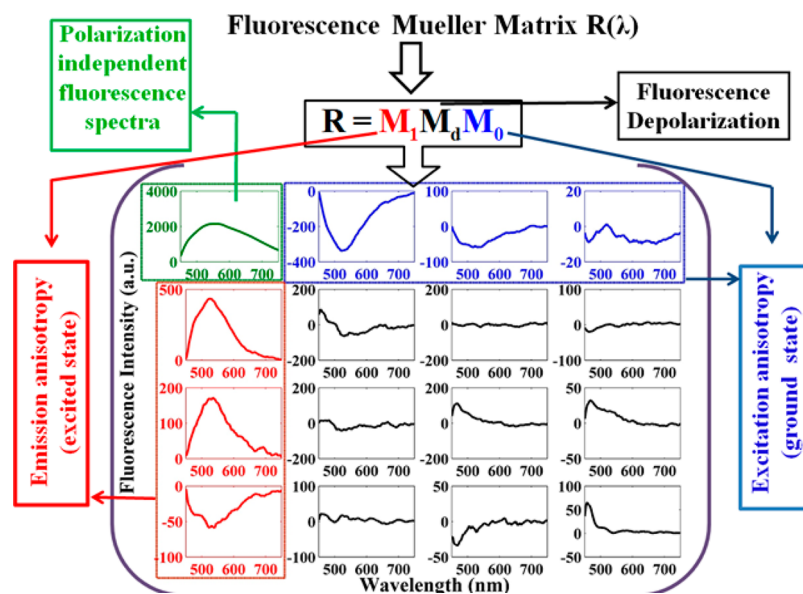


**Figure 4.**  $4 \times 4$  fluorescence spectroscopic Mueller matrix  $\mathbf{R}$  ( $\lambda_{em} = 450\text{--}800$  nm) recorded from painted supramolecular helix from the assembly of a dipeptide and naphthalene-diimide (TB-NDI). The first element ( $R_{11}$ ) represents the polarization independent fluorescence spectra. The other three elements in the first row (blue colored) represent excitation anisotropy related to the ground molecular state while the three elements in the first column (red colored) represent emission anisotropy related to the excited molecular state, respectively.

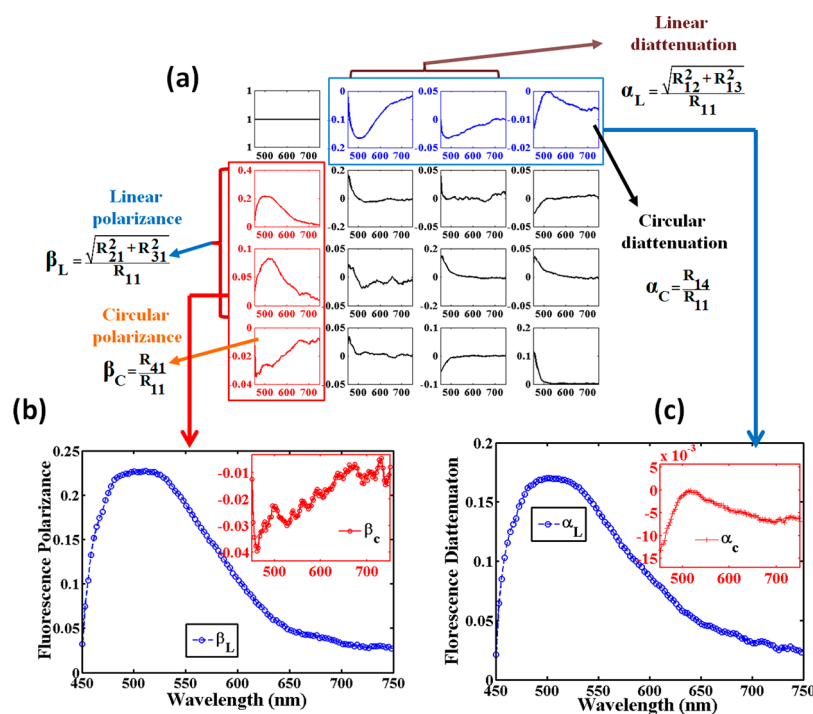


**Figure 5.** (a) Normalized (by the  $R_{11}$  element) fluorescence spectroscopic Mueller matrix. The excitation anisotropies of the ground molecular state quantified through: fluorescence linear ( $\alpha_L$ ) and circular ( $\alpha_C$ ) diattenuation parameters are noted. The emission anisotropies of the excited molecular state quantified through fluorescence linear ( $\beta_L$ ) and circular ( $\beta_C$ ) polarizance parameters are also noted. The corresponding wavelength variation of the magnitudes of (b) emission anisotropies of  $\beta_L$  and  $\beta_C$  and (c) excitation anisotropies  $\alpha_L$  and  $\alpha_C$  are displayed.

red color) of the recorded fluorescence Mueller matrix reflect emission anisotropy of the excited state (differential emission of fluorescence by orthogonal linear and circular polarizations, see the [Experimental Section](#)). The fact that the information on “true” molecular organizational anisotropy is encoded in the elements of the first row and the first column of the fluorescence spectroscopic Mueller matrix was confirmed further by carrying out measurements on a dilute solution of the fluorophores alone, where no such organizational anisotropy effects are expected. In conformity with this, the  $R_{12}$ ,  $R_{13}$ , and  $R_{14}$  (and  $R_{21}$ ,  $R_{31}$ , and  $R_{41}$ ) elements recorded from such solution did not exhibit appreciable intensity values and characteristic spectral shape. In order to now extract quantitative information on such molecular organizational anisotropy, we now resort to the inverse analysis of the fluorescence Mueller matrix.<sup>29</sup>

The recorded fluorescence Mueller matrix (of [Figure 4](#)) is subsequently used to quantify the excitation and the emission anisotropies. The results are presented in [Figure 5](#). For the convenience of interpretation of the anisotropy parameters, in [Figure 5](#), we have shown the normalized (by the  $R_{11}$  element) fluorescence Mueller matrix. The anisotropy parameters are parametrized and quantified via the fluorescence polarizance (linear and circular:  $\beta_L$  and  $\beta_C$ ) and fluorescence diattenuation (linear and circular:  $\alpha_L$  and  $\alpha_C$ ) parameters (see [eqs 6](#) and [7](#) for the definition of the parameters). The spectral variations of these parameters are shown in [Figure 5b,c](#), respectively. As is apparent from the figure, the linear anisotropy parameters of both the ground (reflected as diattenuation effect) and the excited (reflected as polarizance effect) states have considerable magnitudes. As noted above, the fluorescence linear diattenuation  $\alpha_L$  (representing differential excitation of fluorescence by orthogonal linear polarizations) and linear polarizance  $\beta_L$

(differential emission of fluorescence by orthogonal linear polarizations) are exclusively related to preferential (anisotropic) alignment and organization of the fluorophore molecules. In the present case, the parallelly aligned dipeptide molecules grow in a supramolecular tape-like structure. The tape then twists to form a helical tape, which subsequently close into a nanotube. Note that the base compound is not fluorescent in nature. When the electron deficient TB-NDI fluorescent dye is added, its molecules get attached to the sulfur atoms of the base compound, which are also aligned parallel in a tape-like form and then twisted helically along the tubes. Thus, these methionine sulphurs work as hot spots and help to stabilize the electron deficient fluorescent molecules around the tube. The resulting anisotropic organization of the fluorescence molecules are manifested as both fluorescence diattenuation and polarizance effects. Specifically, the parallel aligned supramolecular tape-like structure leaves its dominant signature as considerably high magnitudes of fluorescence linear diattenuation ( $\alpha_L$ ) and fluorescence linear polarizance ( $\beta_L$ ) parameters. Even though, the corresponding circular anisotropy parameters, fluorescence circular diattenuation ( $\alpha_C$ ) and circular polarizance ( $\beta_C$ ) are relatively weaker, they still have nonzero magnitudes and characteristics spectral variation. The observed nonzero magnitudes of the circular anisotropy parameters are in conformity with the circular dichroism (CD) spectroscopic measurements, which also exhibited a Cotton effect as a manifestation of circular anisotropy (see [Figure 2](#)). These parameters therefore provide evidence of the helical arrangement of the fluorescent paint molecules around the supramolecular tubular nanotubes.

The wavelength variation of the average fluorescent dipolar orientation angles for the ground ( $\theta_{ex}$ ) and the excited ( $\theta_{em}$ ) molecular states determined using [eq 8](#) on the experimental

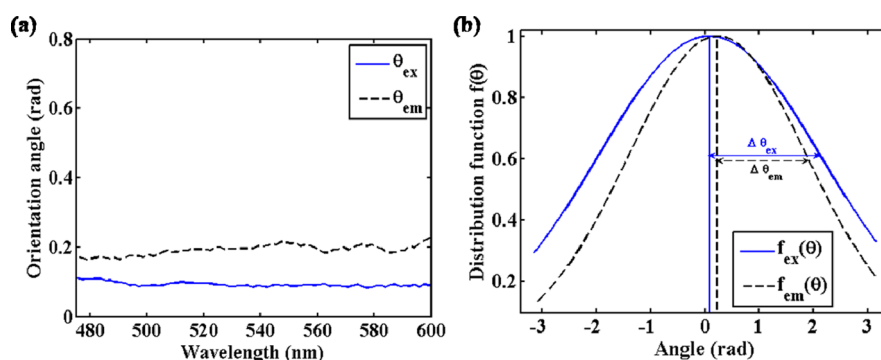


**Figure 6.** (a) Wavelength variation of the average fluorescent dipolar orientation angles for the ground ( $\theta_{\text{ex}}$ , blue solid line) and the excited ( $\theta_{\text{em}}$ , black dashed line) molecular states. (b) The derived molecular angular distribution function for the ground ( $f_{\text{ex}}(\theta)$ , blue solid line)  $\theta_{\text{ex}}$  and the excited ( $f_{\text{em}}(\theta)$ , black dashed line) molecular states of the fluorescent molecule. Inverse calculations using eqs 9–11 were performed on the Mueller matrix-derived  $\alpha_{\text{L}}$  and  $\beta_{\text{L}}$  parameters (at  $\lambda = 510$  nm) to extract this information. The estimated standard deviations of the orientation angle distribution for the ground and excited states were found to be  $\Delta\theta_{\text{ex}} = 0.66\pi$  and  $\Delta\theta_{\text{em}} = 0.53\pi$ , respectively. The vertical lines mark the center positions of the distribution functions.

fluorescence Mueller matrix are shown in Figure 6a. The corresponding results of inverse calculations (using eq 9–11) on the Mueller matrix-derived  $\alpha_{\text{L}}$  and  $\beta_{\text{L}}$  parameters and the resulting information on the molecular angular distribution functions ( $f(\theta)$ ) and its width (representing molecular orientational order) are shown in Figure 6b. The values for the  $\alpha_{\text{L}}$  and  $\beta_{\text{L}}$  parameters at  $\lambda = 510$  nm (0.17 and 0.23, respectively) were used for the inverse calculations. The inverse calculations yielded the values of the standard deviations to be  $\Delta\theta_{\text{ex}} \approx 0.66\pi$  (for the ground state) and  $\Delta\theta_{\text{em}} \approx 0.53\pi$  (excited state) centered around  $\theta_{\text{ex}} \approx 0.08$  rad and  $\theta_{\text{em}} \approx 0.23$  rad (corresponding to Figure 6a). Note that the supramolecular sheet-like structure of the dipeptide and the paint TB-NDI leads to preferential linear organization of the fluorescent molecular dipoles (of TB-NDI), which should lead to considerably high magnitudes of the  $\alpha_{\text{L}}$  and  $\beta_{\text{L}}$  parameters and low values of the  $\Delta\theta_{\text{ex}}$  and  $\Delta\theta_{\text{em}}$  parameters. However, as noted previously, the sheet also twists to form a helical tape, which subsequently closes into nanotube. This 3-dimensional helical arrangement allows a larger range of orientation angles of the dipoles to be probed by excitation of fluorescence with preferential linear polarization (leading to an increase of  $\Delta\theta_{\text{ex}}$ ) or emission of fluorescence with preferential linear polarization (increased  $\Delta\theta_{\text{em}}$ ). Accordingly, the magnitudes of the fluorescence linear diattenuation ( $\alpha_{\text{L}}$ ) and fluorescence linear polarizance ( $\beta_{\text{L}}$ ) parameters are also reduced from their limiting value for the highest molecular order. This helical organization of the molecules are also manifested as nonzero magnitudes of the fluorescence circular diattenuation ( $\alpha_{\text{C}}$ ) and circular polarizance ( $\beta_{\text{C}}$ ) parameters (Figure 5b,c). Thus, the Mueller matrix-derived fluorescence diattenuation and polarizance parameters and their analysis using eqs 8–11 provided useful information on the molecular orientational order of the supramolecular assembly. As previously noted, this information on the molecular orientation order can be treated as an averaged information in space, over the molecular population probed by the excitation light.

## CONCLUSIONS

We have presented a supramolecular nanotube from dipeptide, which is processed with electron deficient organic dyes. The solution and solid state analysis reveal that dipeptides consisting of C-terminal methionine residue felicitate to form

an extended structure and further self-assembled to form supramolecular nanotubes. The methionine sulphurs are arranged helically along the tubes and work as hot spots and help to fix the electron deficient dye TB-NDI around the nanotubes. The Mueller matrix fluorescence spectroscopy can unveil information on the molecular orientation of the supramolecular hybrid. This information was characteristically encoded in various elements of the fluorescence spectroscopic Mueller matrix, which could be gleaned from the inverse analysis. The analysis enabled derivation and quantification of useful information on the formation of decorated supramolecular tubes via a set of fluorescence anisotropy parameters, namely, fluorescence (linear and circular) diattenuation and polarizance. We would like to note that the quantitative link of these newly defined fluorescence anisotropy parameters to the structure, orientation, and organization of molecules is not yet completely developed. The initial analysis presented here established a potentially useful link between these parameters and the molecular orientational order, which could be successfully gleaned. These fluorescence anisotropy parameters therefore hold considerable promise as novel fluorescence metrics for probing and quantifying molecular orientation and shape information. The initial applications of these newly derived fluorescence anisotropy metrics appear promising in this regard and warrant further exploration, which may eventually open the door for characterization of a variety of complex hybrid materials.

## ASSOCIATED CONTENT

### Supporting Information

The Supporting Information is available free of charge on the ACS Publications website at DOI: 10.1021/acs.jpcc.7b06725.

Details of materials, additional figures, and tables as noted in the main text. (PDF)

## AUTHOR INFORMATION

### Corresponding Authors

\*E-mail: nghosh@iiserkol.ac.in.

\*E-mail: deba\_h76@iiserkol.ac.in; deba\_h76@yahoo.com.

### ORCID

Debasish Haldar: 0000-0002-7983-4272



## Notes

The authors declare no competing financial interest.

## ACKNOWLEDGMENTS

K.M. and S.S. thank the IISER-Kolkata, India for a research fellowship. R.D. acknowledges the BRNS-DAE project Govt. of India for funding. We are thankful to Dr. Raju Mandal, I. A. C. S., Jadavpur, Kolkata-700032, India, for his assistance in X-ray crystallography data refinement.

## REFERENCES

- (1) Hamley, I. W. Peptide Nanotubes. *Angew. Chem., Int. Ed.* **2014**, *53*, 6866–6881.
- (2) Seebach, D.; Beck, A. K.; Bierbaum, D. J. The World of  $\beta$ - and  $\gamma$ -Peptides Comprised of Homologated Proteinogenic Amino Acids and Other Components. *Chem. Biodiversity* **2004**, *1*, 1111–1239.
- (3) Babu, S. S.; Praveen, V. K.; Ajayaghosh, A. Functional  $\pi$ -Gelators and Their Applications. *Chem. Rev.* **2014**, *114*, 1973–2129.
- (4) Krieg, E.; Bastings, M. M. C.; Besenius, P.; Rytchinski, B. Supramolecular Polymers in Aqueous Media. *Chem. Rev.* **2016**, *116*, 2414–2477.
- (5) Bhattacharya, S.; Samanta, S. K. Soft-Nanocomposites of Nanoparticles and Nanocarbons With Supramolecular and Polymer Gels and Their Applications. *Chem. Rev.* **2016**, *116*, 11967–12028.
- (6) Yang, L.; Tan, X.; Wang, Z.; Zhang, X. Supramolecular Polymers: Historical Development, Preparation, Characterization, and Functions. *Chem. Rev.* **2015**, *115*, 7196–7239.
- (7) Bong, D. T.; Clark, T. D.; Granja, J. R.; Ghadiri, M. R. Self-Assembling Organic Nanotubes. *Angew. Chem., Int. Ed.* **2001**, *40*, 988–1011.
- (8) Aravinda, S.; Shamala, N.; Roy, R. S.; Balam, P. Non-Protein Amino Acids in Peptide Design. *Proc. - Indian Acad. Sci., Chem. Sci.* **2003**, *115*, 373–400.
- (9) Bowerman, C. J.; Nilsson, B. L. Review Self-Assembly of Amphipathic  $\beta$ -Sheet Peptides: Insights and Applications. *Biopolymers* **2012**, *98*, 169–184.
- (10) Pham, J. D.; Spencer, R. K.; Chen, K. H.; Nowick, J. S. A Fibril-Like Assembly of Oligomers of a Peptide Derived From  $\beta$ -Amyloid. *J. Am. Chem. Soc.* **2014**, *136*, 12682–12690.
- (11) Ghadiri, M. R.; Granja, J. R.; Buehler, L. K. Artificial Transmembrane Ion Channels From Self-Assembling Peptide Nanotubes. *Nature* **1994**, *369*, 301–304.
- (12) Couet, J.; Samuel, J. D. J. S.; Kopyshv, A.; Santer, S.; Biesalski, M. Peptide-Polymer Hybrid Nanotubes. *Angew. Chem., Int. Ed.* **2005**, *44*, 3297–3301.
- (13) Reiriz, C.; Brea, R. J.; Arranz, R.; Carrascosa, J. L.; Garibotti, A.; Manning, B.; Valpuesta, J. M.; Eritja, R.; Castedo, L.; Granja, J. R.  $\alpha$ , $\gamma$ -Peptide Nanotube Templating of One-Dimensional Parallel Fullerene Arrangements. *J. Am. Chem. Soc.* **2009**, *131*, 11335–11337.
- (14) Hourani, R.; Zhang, C.; van der Weegen, R.; Ruiz, L.; Li, C.; Ketten, S.; Helms, B. A.; Xu, T. Processable Cyclic Peptide Nanotubes With Tunable Interiors. *J. Am. Chem. Soc.* **2011**, *133*, 15296–15299.
- (15) Yan, X.; Zhu, P.; Li, J. Self-Assembly and Application of Diphenylalanine-Based Nanostructures. *Chem. Soc. Rev.* **2010**, *39*, 1877–1890.
- (16) Kol, N.; Adler-Abramovich, L.; Barlam, D.; Shneck, R. Z.; Gazit, E.; Rousso, I. Self-Assembled Peptide Nanotubes Are Uniquely Rigid Bioinspired Supramolecular Structures. *Nano Lett.* **2005**, *5*, 1343–1346.
- (17) Adler-Abramovich, L.; Reches, M.; Sedman, V. L.; Allen, S.; Tandler, S. J. B.; Gazit, E. Thermal and Chemical Stability of Diphenylalanine Peptide Nanotubes: Implications for Nanotechnological Applications. *Langmuir* **2006**, *22*, 1313–1320.
- (18) Niu, L.; Chen, X.; Allen, S.; Tandler, S. J. B. Using the Bending Beam Model to Estimate the Elasticity of Diphenylalanine Nanotubes. *Langmuir* **2007**, *23*, 7443–7446.
- (19) Hauser, C. A. E.; Zhang, S. Nanotechnology: Peptides as Biological Semiconductors. *Nature* **2010**, *468*, 516–517.
- (20) Kholkin, A.; Amdursky, N.; Bdikin, I.; Gazit, E.; Rosenman, G. Strong Piezoelectricity in Bioinspired Peptide Nanotubes. *ACS Nano* **2010**, *4*, 610–614.
- (21) Amdursky, N.; Molotskii, M.; Gazit, E.; Rosenman, E. G. Elementary Building Blocks of Self-Assembled Peptide Nanotubes. *J. Am. Chem. Soc.* **2010**, *132*, 15632–15636.
- (22) Görbitz, C. H. The Structure of Nanotubes Formed by Diphenylalanine, the Core Recognition Motif of Alzheimer's  $\beta$ -Amyloid Polypeptide. *Chem. Commun.* **2006**, 2332–2334.
- (23) Reches, M.; Gazit, E. Casting Metal Nanowires Within Discrete Self-Assembled Peptide Nanotubes. *Science* **2003**, *300*, 625–627.
- (24) Morris, K. L.; Zibae, S.; Chen, L.; Goedert, M.; Sikorski, P.; Serpell, L. C. The Structure of Cross- $\beta$  Tapes and Tubes Formed by an Octapeptide,  $\alpha$ S $\beta$ 1. *Angew. Chem., Int. Ed.* **2013**, *52*, 2279–2283.
- (25) Paikar, A.; Pramanik, A.; Das, T.; Haldar, D. A Self-Assembled Peptide Mimetic of a Tubular Host and a Supramolecular Polymer. *Polym. Chem.* **2017**, *8*, 396–403.
- (26) Yu, G.; Jie, K.; Huang, F. Supramolecular Amphiphiles Based on Host-Guest Molecular Recognition Motifs. *Chem. Rev.* **2015**, *115*, 7240–7303.
- (27) Goldstein, D. H. *Polarized Light*; CRC Press: Boca Raton, FL, 2016.
- (28) Arteaga, O.; Nichols, S.; Kahr, B. Mueller Matrices in Fluorescence Scattering. *Opt. Lett.* **2012**, *37*, 2835–2837.
- (29) Saha, S.; Soni, J.; Chandel, S.; Kumar, U.; Ghosh, N. Probing Intrinsic Anisotropies of Fluorescence: Mueller Matrix Approach. *J. Biomed. Opt.* **2015**, *20*, 085005.
- (30) Pramanik, A.; Paikar, A.; Maji, K.; Haldar, D. Photo-Responsive Modulation of Hybrid Peptide Assembly, Charge Transfer Complex Formation and Gelation. *RSC Adv.* **2016**, *6*, 59851–59857.
- (31) Maji, K.; Sarkar, R.; Bera, S.; Haldar, D. A Small Molecule Peptidomimetic of Spider Silk and Webs. *Chem. Commun.* **2014**, *50*, 12749–12752.
- (32) Pramanik, A.; Paikar, A.; Haldar, D. Sonication-Induced Instant Fibrillation and Fluorescent Labeling of Tripeptide Fibers. *RSC Adv.* **2015**, *5*, 53886–53892.
- (33) Soni, J.; Purwar, H.; Lakhota, H.; Chandel, S.; Banerjee, C.; Kumar, U.; Ghosh, N. Quantitative Fluorescence and Elastic Scattering Tissue Polarimetry Using an Eigenvalue Calibrated Spectroscopic Mueller Matrix System. *Opt. Express* **2013**, *21*, 15475–15489.
- (34) Compain, E.; Poirier, S.; Drevillon, B. General and Self-Consistent Method for the Calibration of Polarization Modulators, Polarimeters, and Mueller-Matrix Ellipsometers. *Appl. Opt.* **1999**, *38*, 3490–3502.
- (35) Azzam, R. M. A. Propagation of Partially Polarized Light Through Anisotropic Media With or Without Depolarization: a Differential  $4 \times 4$  Matrix Calculus. *J. Opt. Soc. Am.* **1978**, *68*, 1756–1767.
- (36) Benninger, R. K. P.; Önfelt, B.; Neil, M. A. A.; Davis, D. M.; French, P. M.W. Fluorescence Imaging of Two-Photon Linear Dichroism: Cholesterol Depletion Disrupts Molecular Orientation in Cell Membranes. *Biophys. J.* **2005**, *88*, 609–622.
- (37) Haluska, C. K.; Schröder, A. P.; Didier, P.; Heissler, D.; Duportail, G.; Mély, Y.; Marques, C. M. Combining Fluorescence Lifetime and Polarization Microscopy to Discriminate Phase Separated Domains in Giant Unilamellar Vesicles. *Biophys. J.* **2008**, *95*, 5737–5747.
- (38) Gao, X.; Qiu, W.; Yang, X.; Liu, Y.; Wang, Y.; Zhang, H.; Qi, T.; Liu, Y.; Lu, K.; Du, C.; et al. First Synthesis of 2,3,6,7-Tetrabromonaphthalene Diimide. *Org. Lett.* **2007**, *9*, 3917–3920.
- (39) Sarwar, M. G.; Dragisic, B.; Salsberg, L. J.; Gouliaras, C.; Taylor, M. S. Thermodynamics of Halogen Bonding in Solution: Substituent, Structural, and Solvent Effects. *J. Am. Chem. Soc.* **2010**, *132*, 1646–1653.
- (40) Moretto, V.; Crisma, M.; Bonora, G. M.; Toniolo, C.; Balam, H.; Balam, P. Comparison of the Effect of Five Guest Residues on the  $\beta$ -Sheet Conformation of Host (L-Val) $_n$  Oligopeptides. *Macromolecules* **1989**, *22*, 2939–2944.